Supplementary Material for

B. P. Weiss et al. (2015) Pervasive Remagnetization of Detrital Zircon Host Rocks in the Jack Hills, Western Australia and Implications for Records of the Early Geodynamo, *Earth Planet Sci. Lett.*

A. Thermal and deformational events in the Jack Hills

There were at least three major phases of metamorphism and deformation that affected the association 3 rocks of the Jack Hills. The first major event is thought to be associated with the collision of the Narryer terrane with the adjacent Younami terrane (Myers, 1995), estimated to be complete by ~2600 Ma. Evidence for this event includes intrusive contacts between 2654 ± 7 Ma monzogranite (Pidgeon and Wilde, 1998) and associations 1 and 2 and 2654 ± 5 Ma U-Pb ages for metamorphic monazite in the matrix of Erawandoo Hill pebble conglomerate and as inclusions in Erawandoo Hill detrital zircons. Monazite-xenotime thermometry on Erawandoo Hill samples indicates temperatures reached ~430-470°C at 2653 ± 5 Ma, consistent with 346-487°C temperatures estimated using Ti-in-quartz thermometry (Rasmussen et al., 2010). Thus, although the intrusive contacts between association 3 rocks and the monzogranite are unclear, it is clear that the intrusion postdated deposition of, and by implication metamorphosed, the Erawandoo Hill conglomerate and is likely responsible for the observed greenschist facies mineralogy.

The second event is thought to be associated with the Glenburgh orogeny (collision of Pilboyne and Yilgarn cratons) at 1960-2005 Ma, manifested as inferred 300-500°C thermal disturbances of hornblende and muscovite $^{40}Ar/^{39}Ar$ age spectra (Spaggiari et al., 2008). The third event is thought to be associated with the Capricorn orogeny (intracratonic working of the West Australia craton), manifested as large-scale east–west-trending dextral shearing, 1738-1828 Ma $^{40}Ar/^{39}Ar$ muscovite and biotite ages throughout much of the Jack Hills (Spaggiari et al., 2008), and 1820 ± 25 Ma U-Pb ages for secondary xenotime in association 1 rocks (Rasmussen et al., 2010). Later lower grade disturbances of unknown ages are manifested as kink and conjugate-style folding, faulting and fault reactivation (Spaggiari, 2007).

The last phases of major metamorphism are thought to be associated with the intrusion of dykes associated with the Marnda Moorn and Warakurna large igneous provinces (LIPs) at ~1210 and ~1070 Ma, respectively (Wang et al., 2014; Wingate et al., 2004). Evidence for the latter disturbances include 1130 ± 130 radiation damage ages for Erawandoo Hill detrital zircons (Pidgeon, 2014) [indicating peak temperatures of at least 230 ± 25°C], 980 ± 150 Ma U-Pb discordia lower intercept ages for Jack Hills monzogranite (Pidgeon, 1992), and muscovite $^{40}Ar/^{39}Ar$ laser probe ages indicating a disturbance at ≤1172 Ma (Spaggiari et al., 2008). A final disturbance at ~800 Ma has been recognized from U-Pb ages of monazite and xenotime in the Erawandoo Hill conglomerate (Rasmussen et al., 2010; Rasmussen et al., 2011).

B. Additional rock magnetic experiments.

B.1. High-temperature low-field susceptibility. We measured temperature-dependent susceptibility for powders generated from six cobble clasts in a field of 0.9 mT from room-temperature up to temperatures as high as 700°C. Cobbles were heated in either air or Ar up to various peak temperatures, with some subsamples subjected to multiple heating and cooling cycles to progressively higher peak temperatures. All measurements were acquired with an AGICO MFK1-FA Kappabridge in the UC Santa Cruz Paleomagnetism Laboratory.

During our Kappabridge experiments conducted in air, only one of the six cobbles (D112l) exhibited susceptibility well above the instrument noise limit. For this sample, we observed a susceptibility peak during warming at ~500°C followed by a prominent drop in susceptibility around the magnetite Curie point (compare Fig. 3A with 3C, F and Fig. S1D). The rise and fall in susceptibility during warming and much higher susceptibility during cooling suggests that much of this magnetite was produced by oxidation during the experiment, possibly from sulfides as has been previously observed (Li and Zhang, 2005; Tudryn and Tucholka, 2004; Wang et al., 2008). Cobbles D112k, D112l and W026 also exhibited a small drop in remanence around the hematite Néel point in both air and Ar (Fig. 3A, B, F and Fig. S1B, C). We observed no indication of pyrrhotite's Néel temperature in susceptibility measurements of any sample.

These results differ from the cobble susceptibility measurements by Tarduno and Cottrell (2013). For most of their samples, heating in air led to a pronounced drop in susceptibility around the magnetite Curie point and only mild irreversibility; by comparison only one of our samples showed a strong susceptibility signal in air, while this sample altered significantly (Fig. 3A). Although two of Tarduno and Cottrell (2013)'s other samples did show susceptibility peaks around the magnetite Curie point and irreversibility similar to the results of our Ar heating experiments (Fig. 3E, G and Fig. S1D), their heating experiments in Ar produced susceptibility peaks around pyrrhotite's Curie point (unlike the production of magnetite observed in our Ar experiments; e.g., Fig. 3B, E, G). These results collectively suggest that unlike the cobbles of Tarduno and Cottrell (2013), our fresh cobbles have significant quantities of hematite and goethite and much less magnetite.

B.2. Low-temperature saturation remanence. Low temperature cycling experiments were conducted on fresh cobbles as well as subsamples of cobbles previously subjected to the Kappabridge high-temperature susceptibility measurements. Samples were exposed to a 5 T pulse field at room temperature and then cycled down to 20 K and back up to room temperature in a near-zero field environment using a Magnetic Properties Measurement System (MPMS) 2 equipped with the ultra low field option at the Institute of Rock Magnetism, U. Minnesota.

Our low-temperature cycling of fresh cobble sample D112l identified the 32 K Besnus transition diagnostic of monoclinic pyrrhotite as well as a weaker ~120 K Verwey transition diagnostic of near-stoichiometric magnetite [see (Dunlop and Özdemir, 1997)] (Fig. 3E). However, low-temperature cycling of D112l subsamples previously been heated in air and Ar showed that the Besnus transition had been destroyed while the 120 K transition was strongly enhanced (Fig. 3F), with the remanence having increased by an order of magnitude. These results provide more evidence that the Kappabridge measurements altered the samples leading to the production of magnetite and additionally show that pyrrhotite was destroyed. Given the abundance of pyrrhotite and the paucity of magnetite in these samples as indicated by the MPMS measurements, thermal demagnetization of IRM (main text Section 3.2), and electron microscopy (main text Section 3.4), it is clear that high-temperature susceptibility experiments are insensitive to the presence of pyrrhotite relative to magnetite in the Jack Hills cobbles.

B.3. Room temperature hysteresis and back field isothermal remanence (IRM). Hysteresis measurements were acquired with a Lakeshore Model 668 Vibrating Sample Magnetometer (VSM) in the laboratory of F. Hellman at UC Berkeley. Many samples exhibited strong paramagnetic behavior; the high-field slope of each hysteresis loop was used to estimate the

contribution of paramagnetic and diamagnetic minerals and isolate the ferromagnetic components (Fig. S3).

A Dunlop-Day plot (Dunlop, 2002) suggests that the mean grain sizes of the samples ranges from pseudo single domain to single domain. Although this plot is useful for characterizing most of the samples, it is likely misleading for the monzogranites. Although the plot suggests that the monzogranites contain mixtures of single domain and superparamagnetic grains, the wasp-waisted shapes of their hysteresis loops (Fig. S3D) and their low S-ratios (the IRM in a backfield of 0.3 T divided by IRM acquired in 1.5 T field) of 0.11-0.54, along with the evidence for magnetite, hematite and goethite in monzogranite thermal demagnetization of IRM data (Figs. 2A and S1A), suggest that they are instead likely mixtures of multidomain magnetite and single domain hematite and goethite [see Roberts et al. (1995)].

C. U-Pb geochronology

C.1. Sample and methods

Prismatic zircon crystals were separated from a sample of Erawandoo Hill dolerite (sample Dol6) by standard heavy mineral separation techniques using high-density liquids. Dolerite zircons had undergone variable degrees of metamictization due to sustained radiation damage, as manifested by their turbid colors (Fig. S4) and physical fragility. Four single zircons were selected based on grain morphology and clarity, and analyzed by the U-Pb isotope dilution thermal-ionization mass spectrometry (ID-TIMS) technique following the general procedures described in Ramezani et al. (2011). All zircons were pre-treated prior to dissolution by a chemical abrasion (CA-TIMS) method modified after Mattinson (2005) to mitigate the effects of radiation-induced Pb loss, and were subsequently spiked with the EARTHTIME ET535 mixed ^{205}Pb-^{233}U-^{235}U tracer prior to dissolution and analysis. Chemical abrasion involved thermal annealing of zircons in a furnace at 900°C for 60 hours, followed by leaching in concentrated HF at 180°C for 5 hours. Because of significant metamictization, the Dol6 zircons would not withstand the more intensive leach schedule typically applied to Phanerozoic zircons (11 to 13 hours at 210°C). Isotopic measurements of U and Pb were made on a VG Sector 54 multi-collector mass spectrometer equipped with a Daly ion-counting system. Data reduction including date calculation and propagation of uncertainties was carried out using computer applications and algorithms of Bowring et al. (2011) and McLean et al. (2011). Complete U-Pb data appear in Table S1.

For Mesoproterozoic and older zircons, the generally high precision of the ^{207}Pb/^{206}Pb dates (relative to the corresponding Pb/U dates) and their relative insensitivity to modern Pb loss renders them reliable estimates of the zircon crystallization age. The estimation of a crystallization age for this sample is thus based on the weighted mean ^{207}Pb/^{206}Pb date of a coherent cluster of zircon analyses for which dispersion in the data can be explained by analytical uncertainties alone. Weighted mean date uncertainties are reported at 95% confidence level and follow the notation ±X/Y/Z Ma, where X is the internal (analytical) uncertainty in the absence of all external errors, Y incorporates the U-Pb tracer calibration error and Z includes the latter as well as the decay constant errors of Jaffey et al. (1971). Incorporation of tracer calibration error (Y) is necessary for comparison between data from different techniques, such as ID-TIMS versus sensitive high-resolution ion microprobe (SHRIMP).

C.2. Results

Four zircons analyzed from sample Dol6 yield a discordant array with $^{206}Pb/^{238}U$ dates that range from 1069.59 ± 0.99 Ma to 1079.7 ± 3.0 Ma (Fig. S5) and are likely best explained by variable degrees of Pb loss (see above). Nevertheless, their $^{207}Pb/^{206}Pb$ dates yield a weighted mean of 1078.4 ± 3.4/4.4/6.6 Ma and a MSWD of 0.036. This date represents the best estimate for the emplacement of the dolerite dyke within the supracrustal rocks. The emplacement age of the Erawandoo Hill dolerite overlaps with the estimates for the timing of magmatism associated with the Warakurna large igneous province in west-central Australia (1052 ± 11 to 1078 ± 5 Ma) based on SHRIMP U-Pb zircon geochronology (Wingate et al., 2004).

D. More details about component naming

The component names were assigned based on the range of observed demagnetization temperatures and coercivities in a given sample. Because we are using this notation for components from a diversity of sample lithologies from around the Jack Hills, components with the same name but identified at different sites may not always have the same direction and origin. For example, monzogranite HT components (Section 4.3) persist during thermal demagnetization to several hundred °C higher temperatures and have different directions from HT components identified from the cobble conglomerates (Section 5.2), indicating a different remanence carrier. Furthermore, components with the same name from a single site may even have a diverse origin, particularly for the cobble conglomerate samples for which little stable NRM was observed.

Supplementary Figures

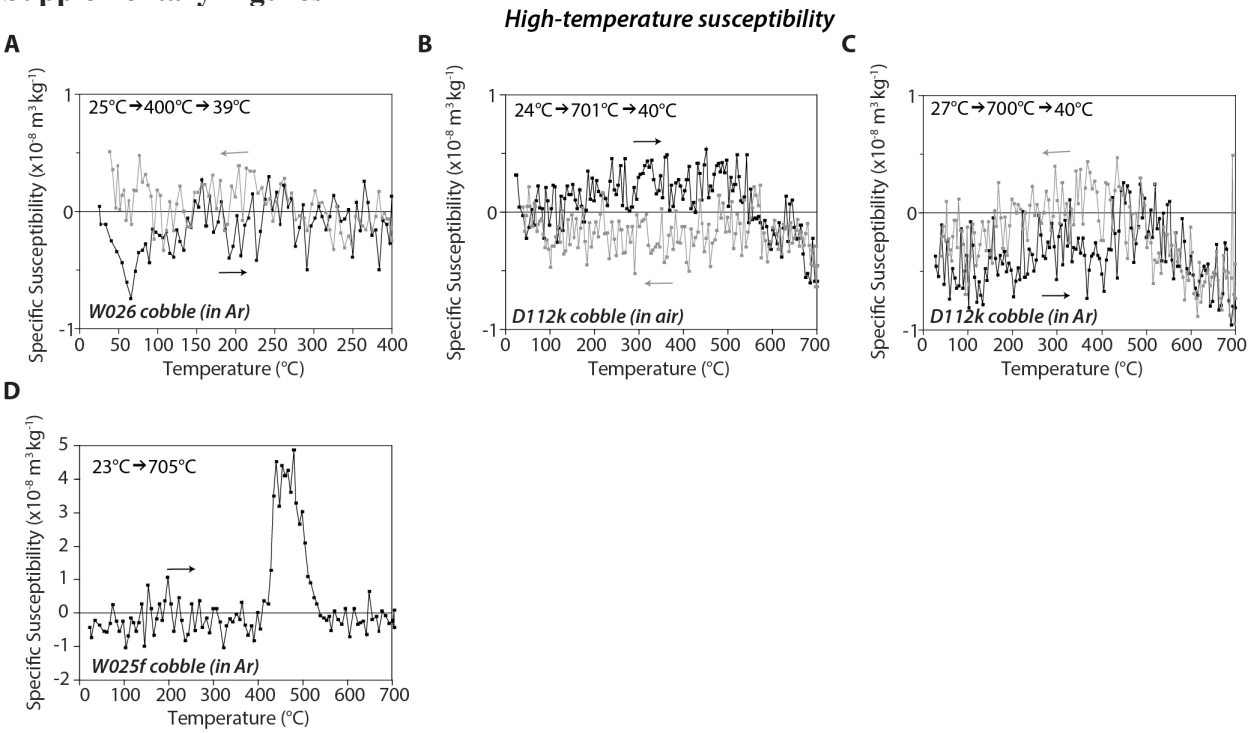

Fig. S1. High temperature susceptibility data. (A) W026 cycled in Ar cycled up to 400°C. (B) D112k cycled in air cycled up to 701°C. (B) D112k cycled in Ar cycled up to 700°C. (D) W025f cycled in Ar cycled up to 705°C.

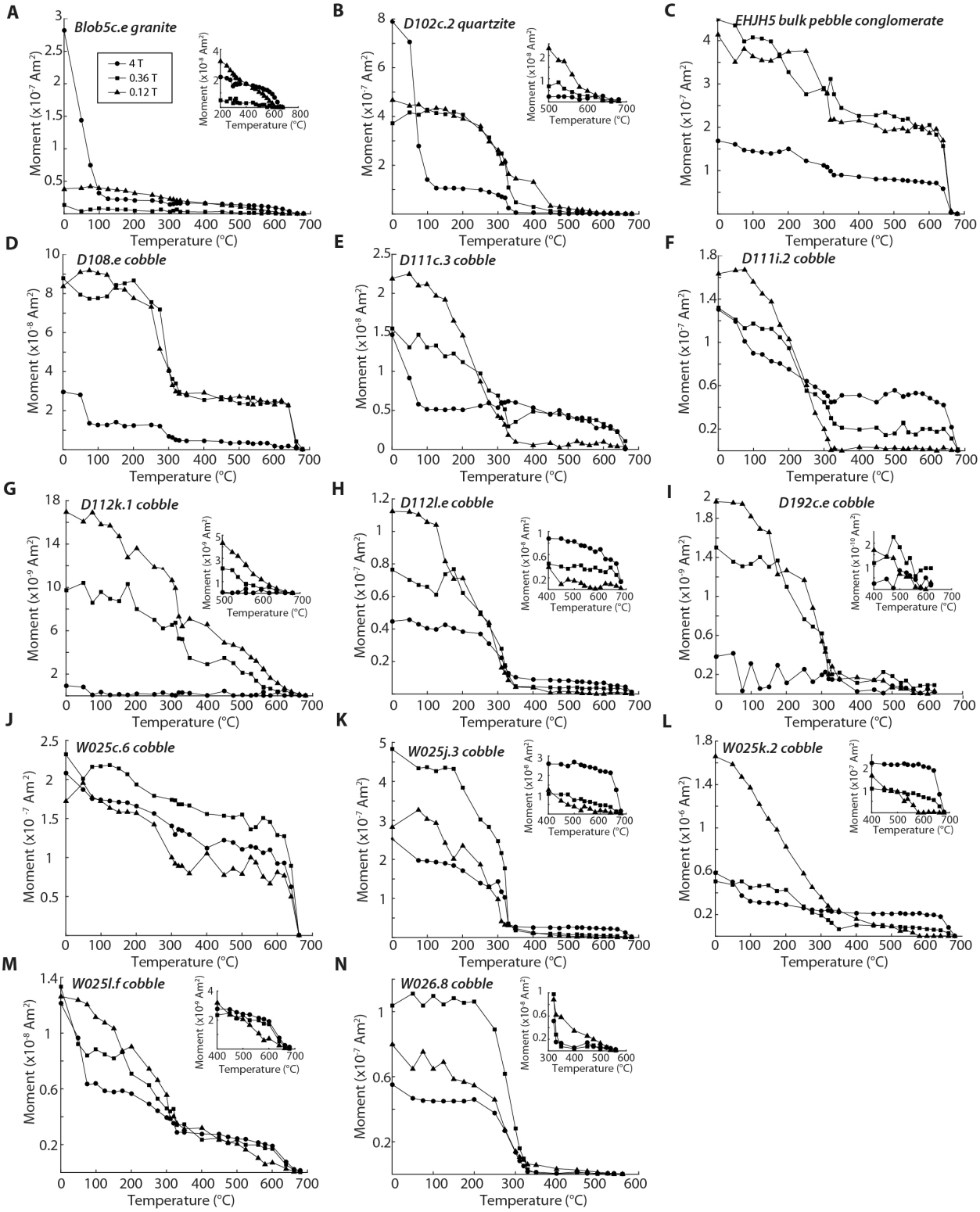

Fig. S2. More examples of thermal demagnetization of a three-component IRM produced by magnetizing the sample in a 4 T field along the *z*-axis, followed by 0.36 T along the north *x*-axis, and 0.12 T along the *y*-axis. Each plot contains curves showing the corresponding *z*- (circles), *y*- (squares), and *x*- (triangles) magnetization components. (A) Granite sample Blob5c.e. (B) Quartzitic fold test sample D102c.2. (C) Bulk sample (clast and matrix) from Erawandoo Hill

pebble conglomerate EHJH5. (D) Clast from cobble conglomerate D108.e. (E) Clast from cobble conglomerate D111c.3. (F) Clast from cobble conglomerate D111i.2 (G) Clast from cobble conglomerate D112k.1. (H) Clast from cobble conglomerate D112l.e. (I) Clast from cobble conglomerate D192c.e. (J) Clast from cobble conglomerate W025c.6. (K) Clast from cobble conglomerate W025j.3. (L) Clast from cobble conglomerate W025k.2. (M) Clast from cobble conglomerate W025l.f. (N) Clast from cobble conglomerate W026.

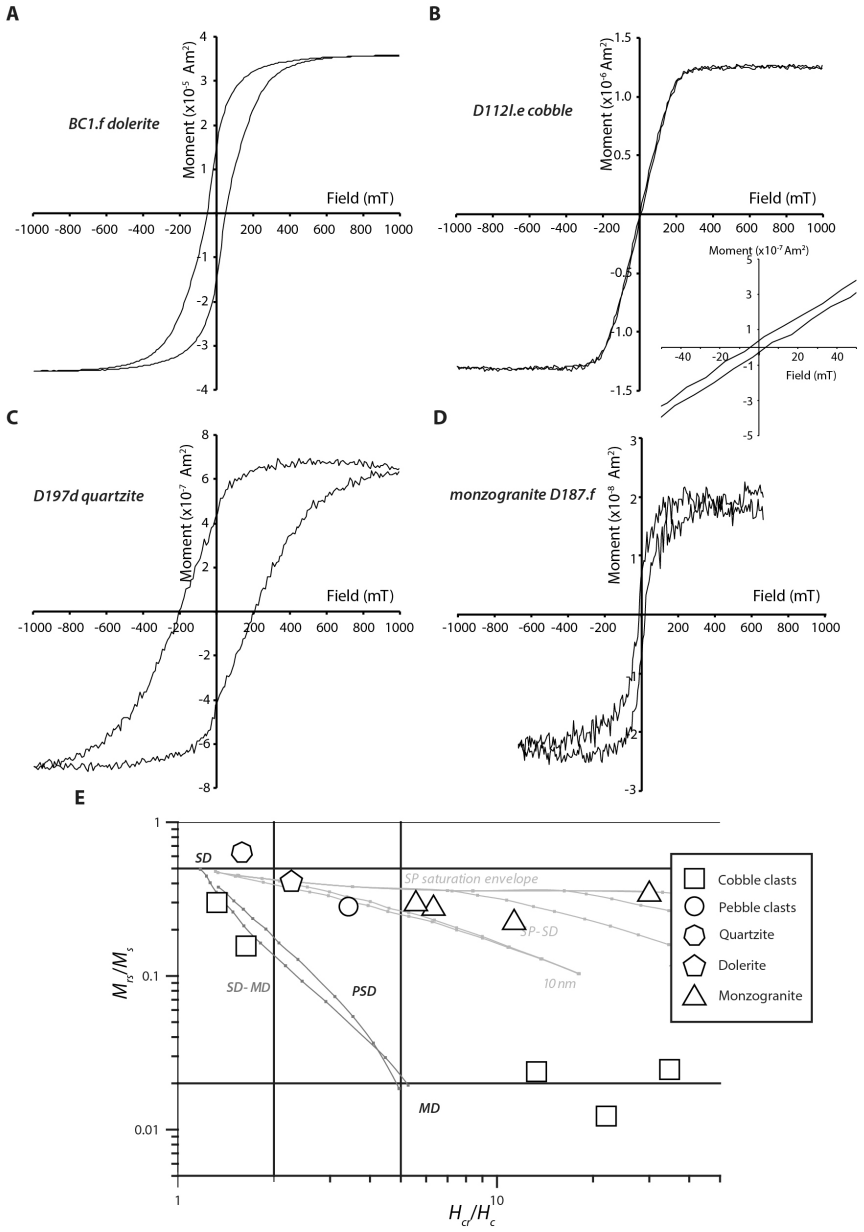

Fig. S3. Room-temperature hysteresis properties of selected samples. (A-D) Room temperature hysteresis loops for dolerite BC1.f (A), clast from cobble conglomerate D112l.e (B), quartzite from fold test D197d (C), and monozogranite D187.f (D). Paramagnetic contributions have been removed from these loops. (E) Dunlop-Day plot (Dunlop, 2002) showing the ratio of coercivity of remanence to coercivity (H_{cr}/H_c) versus the ratio of saturation remanence to saturation magnetization (M_{rs}/M_s) for all samples that yielded low-noise hysteresis loops. Single domain

(SD), pseudo single domain (PSD) and multidomain (MD) ranges calculated for magnetite are indicated, as well as mixing lines between SD and MD and between SD and superparamagnetic (SP) of different sizes are also indicated. Lithologies of samples are denoted by squares for cobbles, circles for pebbles, heptagons for quartzite, pentagons for dolerite, and triangles for monzogranite.

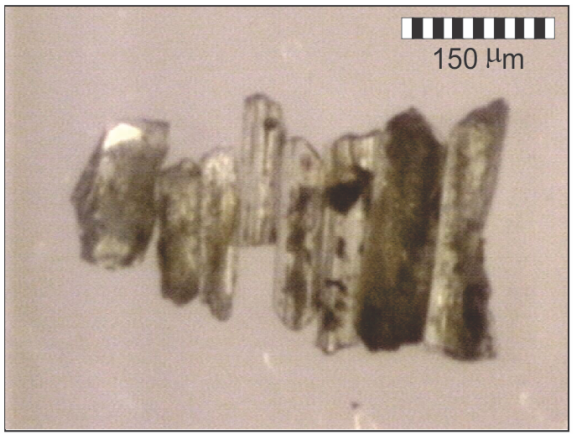

Fig. S4. Photomicrograph of selected zircon grains for U-Pb analysis from dolerite sample Dol6.

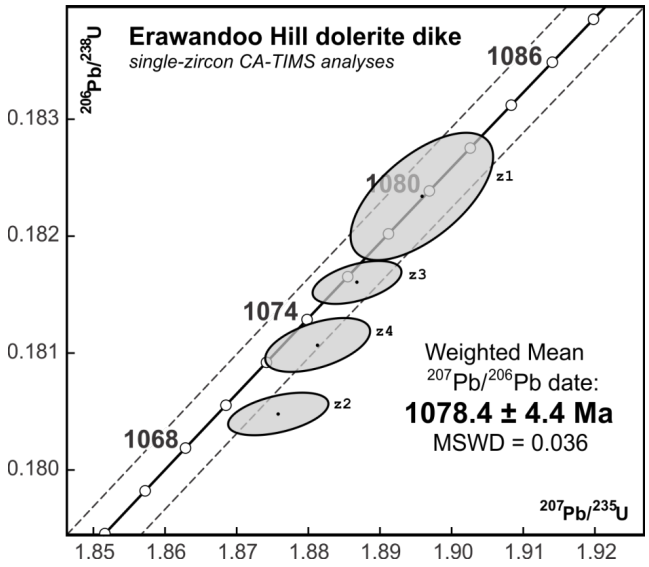

Fig. S5. U-Pb concordia plot for Dol6 dolerite sample with individual analyses of zircon shown with 2σ error ellipses. Uncertainty of the weighted mean date includes all sources of internal (analytical) error as well as the U-Pb tracer calibration error, reported at 95% confidence. Dashed lines mark the concordia error envelope. Complete U-Pb isotopic data are reported in Table S1. MSWD is mean square of weighted deviates.

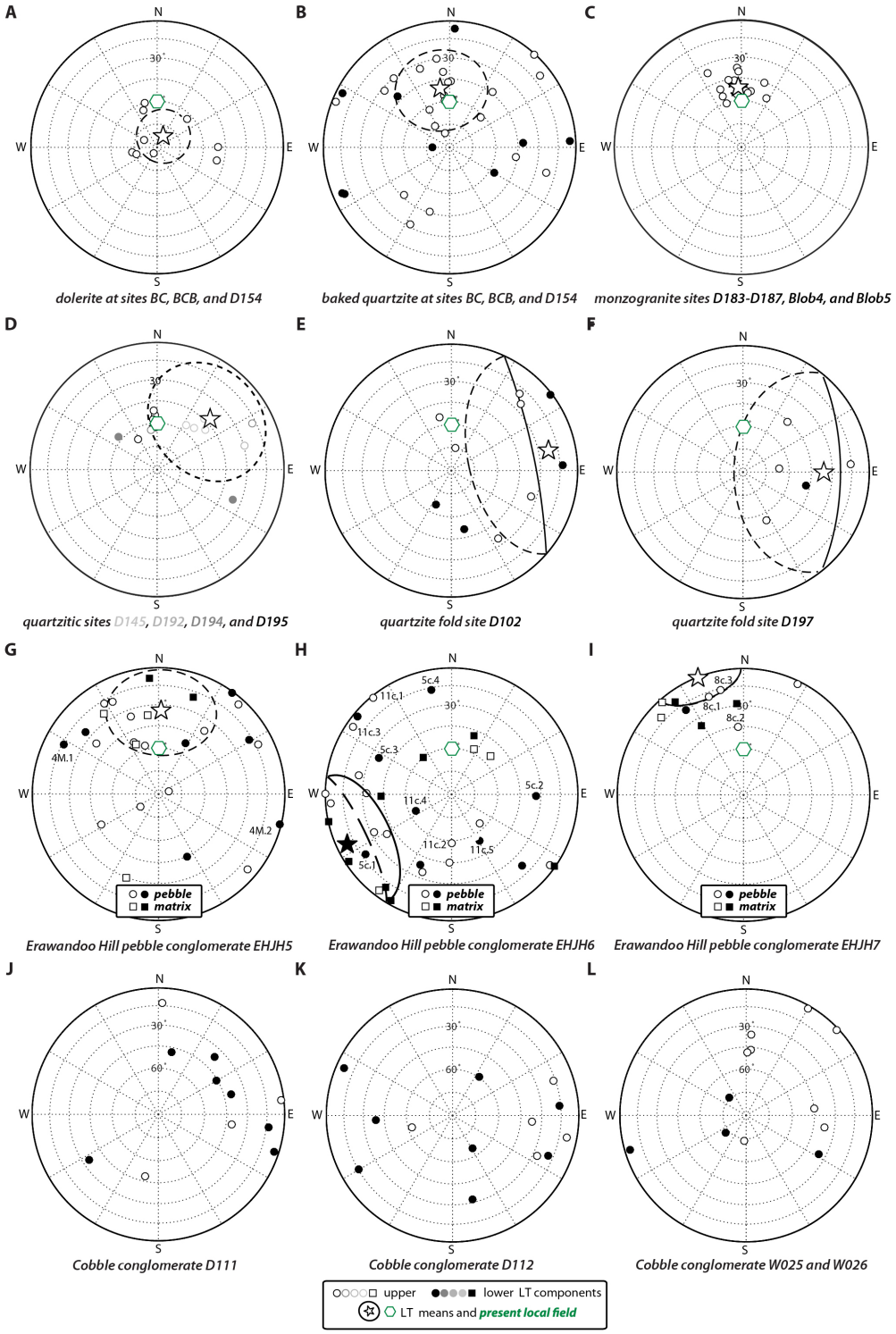

Fig. S6. Equal area stereonets showing LT components. Open and closed symbols represent upper and lower hemispheres. Stars and associated ellipses denote Fisher LT mean directions and associated 95% confidence ellipses for each plot. Green hexagon denotes local geomagnetic field direction. (A) Dolerite at baked contact test sites BC, BCB, and D154. (B) Quartzite at dolerite baked contact test sites BC, BCB, and D154. (C) Monzogranite at sites D183-D187, Blob4, and Blob5. (D) Quartzite at site D145, D192, D194, and D195. (E) Quartzite at fold test

site D102. (F) Quartzite at fold test site D197. (G) Clasts and matrix from Erawandoo Hill pebble conglomerate EHJH5. (H) Clasts and matrix from Erawandoo Hill pebble conglomerate EHJH6. (I) Clasts and matrix from Erawandoo Hill pebble conglomerate EHJH7. (J) Clasts from cobble conglomerate at site D111. (K) Clasts from cobble conglomerate at site D112. (L) Clasts from cobble conglomerate at sites W025 and W026. In (G-I), circles represent clasts and squares represent matrix.

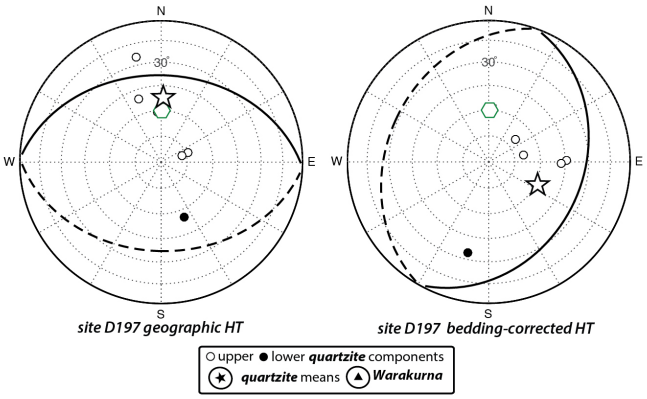

Fig. S7. Equal area stereonets showing HT directions isolate from quartzite samples at fold test site D197 in (A) geographic coordinates and (B) bedding-corrected coordinates. Open and closed symbols represent upper and lower hemispheres. Stars and associated ellipses denote Fisher LT mean directions and associated 95% confidence ellipses for each plot. The mean values do not assume auto-reversal of the one reversed sample. Hexagon denotes local geomagnetic field direction.

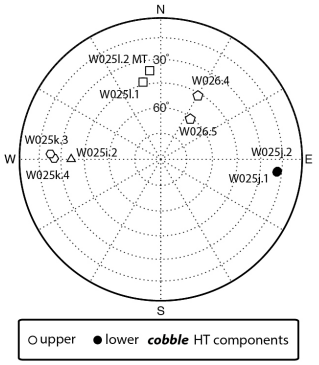

Fig. S8. Equal area stereonet showing HT directions for all W025 and W026 cobbles that yielded linear, origin-trending characteristic components. Subsamples from the same clast are denoted with the same symbol. Open and closed symbols represent upper and lower hemispheres.

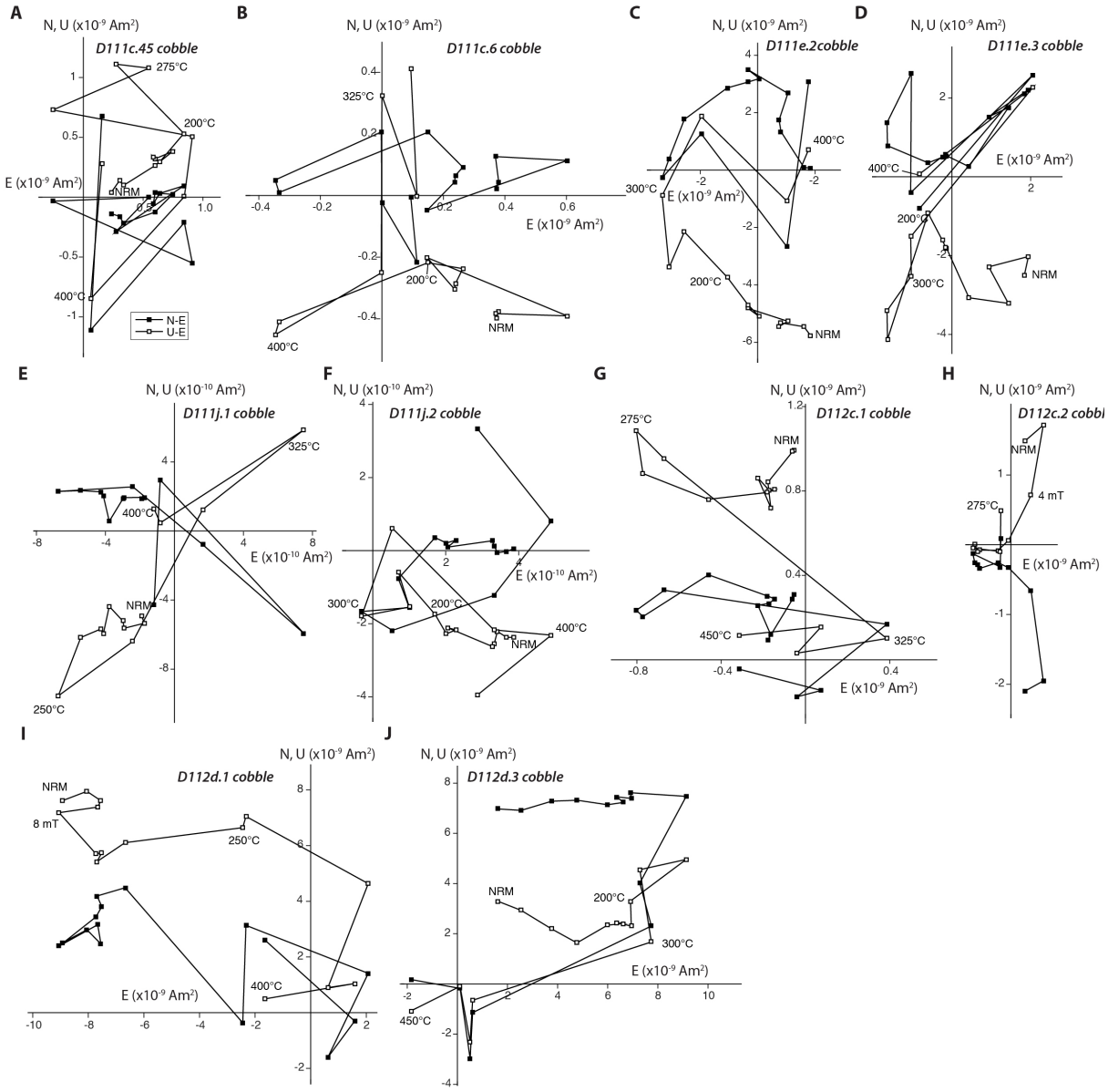

Fig. S9. Paleomagnetism of additional samples from the cobble conglomerate tests. Shown are two-dimensional projections of the endpoint of the NRM vector during AF and thermal demagnetization in geographic coordinates. Open and closed symbols represent end points of magnetization projected onto north-east (N-E) and up-east (U-E) planes, respectively. Peak AC fields and temperatures for selected AF and thermal demagnetization steps are labeled. (A, B) Two subsamples from cobble D111c. (C, D) Two subsamples from cobble D111e. (E, F) Two subsamples from cobble D111j. (G, H) Two subsamples from cobble D112c. (I, J) Two subsamples from cobble D112d.

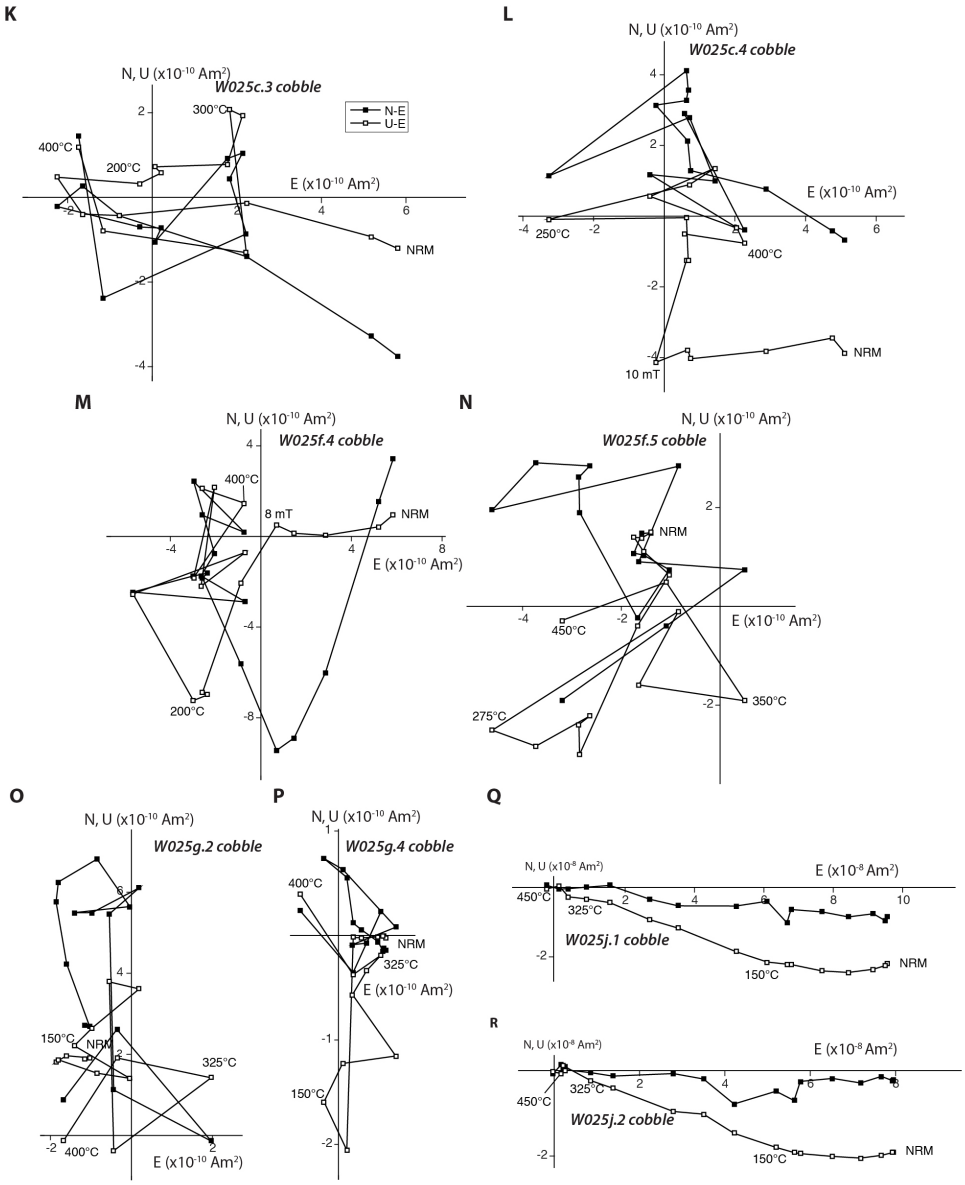

Fig. S9 continued. (K, L) Two subsamples from cobble W025c. (M, N) Two subsamples from cobble W025f. (O, P) Two subsamples from cobble W025g. (Q, R) Two subsamples from cobble W025j.

Table S1. U-Pb data for analyzed zircons from Jack Hills dolerite dyke.

	Composition					Ratios						Dates (Ma)				
Sample	Pb_c[‡]	Pb*[‡]	Th	^{206}Pb[§]	^{208}Pb[#]	^{206}Pb[††]	err	^{207}Pb[††]	err	^{207}Pb[††]	err	^{206}Pb	^{207}Pb	^{207}Pb	err	corr.
Fraction	(pg)	Pb_c	U	^{204}Pb	^{206}Pb	^{238}U	2σ%	^{235}U	2σ%	^{206}Pb	2σ%	^{238}U	^{235}U	^{206}Pb	2σ	coef.
Erawandoo Hill Dolerite Dyke (Dol6)																
z1	0.18	47	1.30	2292.5	0.393	0.182339	(.30)	1.89585	(.52)	0.07544	(.41)	1079.7	1079.6	**1079.4**	**8.3**	0.62
z2	0.24	43	0.94	2275.0	0.285	0.180479	(.10)	1.87581	(.37)	0.07541	(.34)	1069.59	1072.6	**1078.7**	**6.8**	0.48
z3	0.18	62	1.60	2857.0	0.484	0.181604	(.10)	1.88680	(.33)	0.07539	(.29)	1075.7	1076.5	**1077.9**	**5.9**	0.49
z4	0.15	44	0.94	2304.3	0.283	0.181069	(.13)	1.88130	(.39)	0.07539	(.34)	1072.8	1074.5	**1078.0**	**6.9**	0.51

Notes: Corr. coef. = correlation coefficient. Age calculations are based on the decay constants of Jaffey et al. (1971)

[†] All analyses are single zircon grains and pre-treated by the thermal annealing and acid leaching (CA-TIMS) technique. Data used in age calculations are in **bold**.

[‡] Pb_c is total common Pb in analysis. Pb* is radiogenic Pb concentration.

[§] Measured ratio corrected for spike and fractionation only.

[#] Radiogenic Pb ratio.

[††] Corrected for fractionation, spike, blank, and initial Th/U disequilibrium in magma. Mass fractionation correction of 0.25%/amu ± 0.04%/amu (atomic mass unit) was applied to single-collector Daly analyses. All common Pb is assumed to be blank. Total procedural blank was less than 0.1 pg for U. Blank isotopic composition: $^{206}Pb/^{204}Pb$ = 18.42 ± 0.35, $^{207}Pb/^{204}Pb$ =15.36 ± 0.23, $^{208}Pb/^{204}Pb$ = 37.46 ± 0.74.

Table S2. NRM components as identified by principal components analysis (PCA).

Sample	Cp.	Range	O?	δ (°)	i (°)	N	MAD/ α_{95} (°)	Notes
Dolerite:								
BCB1.1	*LT*	*10 mT-80°C*	*N*	*29.8*	*-29.6*	*3*	*3.8*	
	HT	80-440°C	*Y*	*320.1*	*-41.7*	*16*	*5.9*	*Unstable above 480°C*
BC0.1	LT	NRM-175°C	N	46.7	-63.4	8	34.6	
	HT	200-530°C	Y	30.1	23.2	17	1	
BC0.2	LT	NRM-200°C	N	259.2	-73.6	9	10.2	
	HT	225-585°C	Y	30.4	19.6	23	4.9	
BC1.1	LC	NRM-10 mT	N	235.7	-40.9	6	2.8	
	LT	10 mT-150°C	N	89.7	-50.1	6	20	
	HT	150-585°C	Y	27.2	45.4	26	2.2	
BC1.2	LC	NRM-10 mT	N	242	-38.9	6	4.7	
	LT	10 mT-150°C	N	102.4	-50	6	19.7	
	HT	150-585°C	Y	31.8	42.1	26	1.5	
Dol1.1	LC	NRM-4 mT	N	279.7	-3.2	3	1.6	
	HT	4 mT-560°C	Y	10.7	39.3	29	3.7	
Dol2.1	LC	NRM-6 mT	N	183.1	11.3	4	3.9	
	LT	10 mT-200°C	N	251.6	-76	7	14.3	
	MT 1	200-275°C	N	344.8	34	4	4.2	
	MT 2	290-360°C	N	262.8	-41.3	4	8.5	
	HT	400-560°C	Y	1.1	39.8	12	2	
Dol3.1	LC	2-10 mT	N	194.1	0.5	5	3.2	
	LT	10 mT-200°C	N	306.7	-73.9	7	16.8	
	MT 1	200-290°C	N	327.1	44.2	5	4.5	
	MT 2	290-360°C	N	238.6	-47.8	4	29.2	
	HT	440-585°C	Y	356.5	55.2	16	3.4	
Dol3.2	LC	2-10 mT	N	196.3	-1.9	*5*	8.9	
	LT	10 mT-200°C	N	210.2	-85.6	7	14.1	
	MT 1	200-275°C	N	337.3	42.4	*4*	5.7	
	MT 2	275-360°C	N	289.9	-44.8	5	20.2	
	HT	360-585°C	Y	0.8	51.2	17	2.9	
Dol5.1	LT	NRM-200°C	N	339.7	-64.6	12	16.9	
	HT	200-585°C	Y	42.2	56.5	26	2.7	
Dol5.2	LT	NRM-175°C	N	344.4	-60.1	11	29	
	HT	200-530°C	Y	41.1	53.6	17	2	
Dol6.1			*Weathered and with anomalous and self-reversing NRM*					
Dol6.2			*Weathered and with anomalous and self-reversing NRM*					
D154d.1	HT	225-585°C	Y	359.5	64.7	23	2.3	
D154d.2	HT	100-585°C	Y	0.9	65.3	28	1.4	
D154j.1			*Weathered and with anomalous and self-reversing NRM*					

D154j.2				*Weathered and with anomalous and self-reversing NRM*				
Dolerite mean	LT			28	-81.8	9	17.5	Fisher *k* = 8.6
	HT			19.3	47.5	12	10.1	Fisher *k* = 17.9
Baked quartzitic country rock:								
BCB2.1	LT	2 mT-305°C	N	321.1	-30.7	17	11.5	
	HT	320-510°C	Y	35.3	32.7	9	13.8	
BCB3.1	LT	NRM-305°C	N	291.8	-3.3	15	12.8	
	MT	305-400°C	N	245.4	17.7	4	4.2	
	HT	400-480°C	Y	36.7	20.9	5	20.7	
BCB3.2	LT	4 mT-360°C	N	296.8	5.5	18	11.8	
	HT	360-420°C	Y	347.1	66.7	3	15.5	
BCB4.1	LT	6 mT-275°C	N	342	-80.4	13	29.6	
	HT	275-360°C	Y	23.4	59.7	5	14.3	
BCB4.2	LT	8 mT-360°C	N	351.5	-29.3	16	29.8	
	HT	460-560°C	Y	63.5	44.3	8	11.9	
BCB4.3	HT	360-560°C	Y	65.8	35.9	11	8.5	
BCB4.4	HT	360-575°C	Y	59.7	52.0	15	13.8	
BCB5.1	LT	225-305°C	N	246.1	9.9	5	15.8	
	HT	320-565°C	Y	42.6	55.2	14	10.8	
BCB6.1	LT	50-360°C	N	42.4	-0.8	13	32.6	
	HT	360-500°C	Y	351.5	21.1	7	22.4	
BCB6.2	LT	290-420°C	N	87	5.2	6	17	
	HT	420-520°C	Y	39.2	51.2	7	16.6	
BCB7.1				*No stable origin-trending magnetization*				
BCB8.1	*LT*	*NRM-225°C*	*N*	*351.2*	*-55.4*	*14*	*16*	
	MT	*250-320°C*	*N*	*198*	*-11.8*	*5*	*19.9*	
	HT	*360-560°C*	*Y*	*349.4*	*-61.4*	*13*	*17.2*	*Hematite carrier; inhomogeneous with BCB8.2*
BCB8.2	LT	8 mT-200°C	N	327	-73.4	9	9.4	
	HT	275-510°C	Y	27.4	-6.8	12	30.3	
BCB9.1	*HT*	*225-320°C*	*Y*	*41.6*	*57.1*	*6*	*1.3*	*Likely lightning remagnetized*
BCB10.1	LT	4 mT-275°C	N	104.6	-21.9	14	4.9	
	HT	360-575°C	Y	92.5	-18.5	16	8.3	
BCB >3r_{dyke} mean	HT			36.5	14.1	4	65.8	Fisher *k* = 2.0; samples BCB6.1, 6.2, 8.2, and 10.1
BCB 1.2-3r_{dyke} mean	HT			44.9	50.1	7	17.7	Fisher *k* = 11.6; samples BCB3.1, 3.2, 4.1, 4.2, 4.3, 4.4, 5.1
BCB <1.2r_{dyke} mean	HT			35.3	32.7	1		Sample BCB2.1
BC3.1	LT	NRM-100°C	N	223.8	-46.7	9	5.4	
	HT	100-225°C	Y	20.1	33.5	6	14.8	
BC4.1	LC	NRM-8 mT	N	203.4	-42.1	5	4.2	
	LT	50-275°C	N	98.2	-46.1	10	22.9	

	HT	320-585°C	Y	56.5	48.7	17	10.8	
BC4.3	LT	NRM-175°C	N	197.2	-45.7	12	7.1	
	HT	225-585°C	Y	31.2	54.8	23	16.8	
BC4.4	LT	NRM-400°C	N	207.3	-32.1	21	9.2	
	HT	440-550°C	Y	35.4	60.4	9	8.4	
BC5.1	*HT*	*6 mT-560*°C	*Y*	*204.7*	*-25.1*	*29*	*2.5*	*Likely lightning remagnetized*
BC5.2	*HT*	*4 mT-560*°C	*Y*	*203.5*	*-25.6*	*30*	*2.8*	*Likely lightning remagnetized*
BC5.3	*HT*	*6 mT-575*°C	*Y*	*198.7*	*-26.8*	*32*	*1.7*	*Likely lightning remagnetized*
BC5.4	*HT*	*4 mT-565*°C	*Y*	*194*	*-30.4*	*31*	*2*	*Likely lightning remagnetized*
BC6.1	LT	6 mT-250°C	N	86.5	41.3	12	24.2	
	HT	250-500°C	Y	69.4	42.8	12	4.7	
BC7.1	LC	NRM-10 mT	N	269	-29.8	3	7.1	
	LT	10 mT-320°C	N	314.4	41.8	14	35.1	
	HT	320-570°C	Y	19.9	58.9	16	29.2	
BC7.2	LC	NRM-10 mT	N	240.9	5.7	3	8.3	
	LT	10 mT-175°C	N	353.9	-56	7	11.3	
BC8.1	LT	2 mT-360°C	N	2.5	6.6	19	23.5	
	HT	360-560°C	Y	45.1	40.6	13	7.5	
BC9.1	LT	4 mT-305°C	N	119.6	56.6	16	5.9	
	HT	305-560°C	Y	302.6	72.4	15	8.1	
BC10.1	LC	NRM-10 mT	N	250.4	59.8	3	1.6	
	HT	275-320°C	Y	263.9	33.2	4	7	
BC10.2	LC	NRM-10 mT	N	260.7	56.6	3	1.5	
	LT	10 mT-250°C	N	331.8	-62	10	9.8	
	HT	250-360°C	Y	41.7	75.5	6	15.7	
BC >3r_{dyke} mean				*334.4*	*74.2*	*4*	*49.9*	Fisher *k* = 3.0; samples BC8.1, 9.1, 10.1, 10.2
BC 1.2-3r_{dyke} mean				*44.9*	*54.5*	*5*	*13.6*	Fisher *k* = 26.3; samples BC4.1, 4.3, 4.4, 6.1, and 7.2
BC <1.2r_{dyke} mean				*20.1*	*33.5*	*1*		Sample BC3.1
D154a.1	*LC*	*NRM-10 mT*	*N*	*153.9*	*51.2*	*6*	*19.7*	
	LT	*10 mT-225*°C	*N*	*51.3*	*-9.5*	*9*	*12.2*	
	HT	*275-360*°C	*Y*	*170.2*	*-32*	*5*	*6*	*Noisy demagnetization; inhomogeneous with D154a.2*
D154a.2	*LT*	*8 mT-225*°C	*N*	*270.1*	*78.9*	*10*	*16.6*	
	MT	*225-360*°C	*N*	*45.1*	*-75.5*	*7*	*20*	
	HT	*400-570*°C	*Y*	*251*	*78.9*	*12*	*28.4*	*Noisy demagnetization; inhomogeneous with D154a.1*
D154b.1	*LC*	*NRM-6 mT*	*N*	*160.9*	*-5.6*	*4*	*18.8*	
	HT	*6 mT-290*°C	*Y*	*31.4*	*-66.1*	*14*	*9.9*	*Noisy demagnetization*
D154c.1	LC	NRM-10 mT	N	117	3.7	6	31.9	
	LT	50-250°C	N	247.4	9	9	25.9	
	HT	250-290°C	Y	29	11.1	3	10.9	
D154c.2	LC	NRM-6 mT	N	187.3	-39.8	4	11.2	
	HT	6 mT-150°C	Y	66.8	6.9	8	5.2	
D154c.3	LC	NRM-10 mT	N	182	-19	6	15.4	
	LT	50-400°C	N	46.5	-62.3	14	18.9	

	HT	400-500°C	Y	53.7	65.6	5	11.7	
D154e.1	HT	290-565°C	Y	21.2	50.9	17	6.1	
D154e.2	LT	10 mT-440°C	N	311	-32.2	18	24.5	
	HT	440-540°C	Y	26.6	58.9	8	7.1	
D154f.1	LT	NRM-200°C	N	2.9	-58.4	13	3.8	
	HT	320-520°C	Y	29.3	51	10	5.9	
D154g.1	LT	50-360°C	N	37.8	-43.8	14	16.2	
	HT	360-560°C	Y	83.1	51.7	13	20.3	
D154h.1	LT	10 mT-80°C	N	354	-59.5	3	4.7	
	HT	80-200°C	Y	104.1	73.6	5	10.6	Not clearly origin-trending
D154h.2	LT	10 mT-80°C	N	356.5	-59.5	3	3.7	
	HT	150-225°C	Y	80.2	-7.5	4	6.2	
D154i.1	LT	10 mT-275°C	N	339.3	-33.9	11	18.4	
	HT	275-320°C	Y	78	30.1	4	7.7	
D154i.2	LT	10 mT-150°C	N	0.1	-46.4	6	3.1	
	MT	150-275°C	N	117.3	13.9	6	34.7	
	HT	275-305°C	Y	355.7	22.4	3	6.2	
D154i.3	LT	10 mT-80°C	N	355	-39.8	3	3.8	
	HT	150-290°C	Y	44.5	48.5	7	5.4	
D154i.4	LT	10 mT-250°C	N	358.6	-47.2	10	14.9	
	HT	250-305°C	Y	335.2	55.6	4	3.5	
D154 >3r_{dyke} mean	HT			48.5	48.8	8	28.1	Samples D154f, g, h, i; Fisher *k* = 3.9
D154 1.2-3r_{dyke} mean	HT			40.6	40.4	5	31.9	Samples D154c, e; Fisher *k* = 5.4
BC, BCB, and D154 quartzite mean	LT			350.3	-50.7	33	27.6	Fisher *k* = 1.8
Monzogranite:								
D182a.1	LC	NRM-8 mT	N	113.6	22.7	5	14.9	
	HT	10 mT-290°C	Y	342.2	59.4	12	10.4	
D183.1	LT	10 mT-150°C	N	339.9	-50	6	1.3	
	HT	360-560°C	Y	337.2	45.1	13	18.5	
D183.2	LT	10 mT-150°C	N	357.8	-54.7	6	2.4	Using second 150°C step
	HT	150-290°C	Y	340.6	9.6	9	7.2	Using second 150°C step
D184.1	LT	10 mT-150°C	N	355	-57.8	6	4.5	Using second 150°C step
	HT	*150-575°C*	*Y*	*57.9**	*29**	*25*	*25.1*	*Circle fit; hematite carrier; Using second 150°C step*
D185.1	LT	10 mT-80°C	N	19.7	-45.4	3	4.5	
	HT	80-360°C	Y	329.9	72.7	13	10.6	
D185.2	LT	10 mT-80°C	N	341.3	-60.3	3	2.9	
	HT	225-480°C	Y	5.7	55.5	12	10.4	
D186.1	LT	6 mT-225°C	N	354.1	-46.2	10	0.9	
	HT	290-540°C	Y	351.9	4.2	14	10.3	
D187.1	LC	2-10 mT	N	317.4	-17.8	5	5.8	
	LT	10 mT-225°C	N	27.2	-54.5	8	7.4	
	HT	225-500°C	Y	359	28.5	14	8.5	
D187.2	LT	4 mT-200°C	N	355.2	-55.7	10	4.6	

	HT	200-540°C	Y	341.6	19.9	18	7.9	
D187.3	LC	NRM-10 mT	N	344.2	-9.5	6	8.9	
	LT	10 mT-275°C	N	348.7	-60.8	10	3.3	
	HT	275-570°C	Y	0.1	35.4	18	5.6	
D187.4	LT	6 mT-200°C	N	358	-62.7	9	4.6	
	HT	200-540°C	Y	353.9	32.2	18	4.9	
D188.1	*LT*	*10 mT-80°C*	*N*	*134.0*	*-52.3*	*2*		*Low thermal stability, 2 point fit*
	HT	80-305°C	Y	34.8	68.4	11	5	
D188.2	*LT*	*10 mT-80°C*	*N*	*125.7*	*-57.9*	*2*		*Low thermal stability, 2 point fit*
	HT	100-320°C	Y	0.4	69.5	11	5.8	
D189.1	*HT*	*6 mT-585°C*	*Y*	*318*	*-22.5*	*32*	*2.3*	*Likely lightning remagnetized*
D189.2	*HT*	*4 mT-585°C*	*Y*	*313.3*	*-22.2*	*33*	*3.5*	*Likely lightning remagnetized*
Blob4a.1	LT	NRM-200°C	N	356.8	-37.6	12	11	
	HT	200-520°C	Y	302.4	80.1	16	29.1	
Blob4a.2	LT	4 mT-175°C	N	357.8	-40.2	9	11.2	
	HT	175-520°C	Y	30.3	82.1	16	20	
Blob4a.3	LT	4 mT-275°C	N	335.4	-36.3	13	6.6	
	HT	290-510°C	Y	70.1	64.8	11	22.3	
Blob4a.4	LT	4 mT-275°C	N	349.1	-45.4	14	13.1	Using second 100°C step
	MT	275-520°C	N	43.6	36.7	14	21.6	No origin-trending HT component
Blob5b.1	LC	2-10 mT	N	179.5	-18.1	5	4.3	
	HT	100-440°C	Y	16.6	39	15	9.4	
Blob5b.2	LC	2-10 mT	N	178	-19.8	5	5.6	
	LT	*10 mT-250°C*	*N*	*327.9*	*-12.9*	*9*	*22*	*Using third 80°C step*
	HT	250-520°C	Y	16	72.3	14	11.2	
Blob5c.1	LT	2 mT-200°C	N	10.2	-53.1	11	4.8	
	HT	200-520°C	Y	357.2	64.5	16	6.7	Using first 520°C step
Blob5c.2	LT	8 mT-100°C	N	4.5	-53.5	4	1.6	
	HT	*125-150°C*	*Y*	*354.4*	*60.2*	*2*	*12.1*	*Very weak moment by 125°C*
Blob5c.3	LT	2 mT-80°C	N	6.8	-54.7	6	4.2	
	HT	150-510°C	Y	17.3	42.3	15	5.5	
Monzogranite mean	LT			357.2	-51.9	17	5.2	Fisher k = 48.3
	HT			358	51.9	19	11.7	Fisher k = 9.2

Quartzitic country rock:

D145.1	LT	2 mT-305°C	N	42.9	-44.6	17	5.2	
	HT	*305-420°C*	*Y*	*341.5*	*-55.5*	*5*	*7.3*	*Hematite carrier; present field direction*
D145.2	LT	4 mT-275°C	N	50.5	-49.3	14	9.4	
	HT	*275-400°C*	*Y*	*351.6*	*-39.2*	*6*	*5.4*	*Hematite carrier; present field direction*
D145.3	LT	2 mT-80°C	N	41.6	-53.9	7	4.6	
	HT	*80-360°C*	*Y*	*4.4*	*-49.2*	*13*	*4.7*	*Hematite carrier; present field direction*
D145.4	LT	4 mT-320°C	N	33.1	-55.6	17	7.1	

	HT	*320-520°C*	*Y*	*337.1*	*-43.5*	*10*	*9.6*	*Hematite carrier; present field direction*
D192b.1	LC	NRM-6 mT	N	338.6	6.1	3	3.9	*Noisy demagnetization*
	LT	*6 mT-250°C*	*N*	*136.9*	*-1.6*	*11*	*30.6*	
	HT	250-320°C	Y	15.4	38.7	5	36	
D192b.2	LC	NRM-6 mT	N	312.9	-10.4	4	33.5	
	LT	6 mT-225°C	N	74.7	-29.4	10	16.9	
	HT	225-360°C	Y	343.7	77.9	7	19.2	
D194b.1	LT	NRM-225°C	N	116.6	35.5	12	32.9	No origin-trending HT component
D194b.2	LT	150-225°C	N	310.5	57.3	4	18	No origin-trending HT component
D194b.3	LC	NRM-10 mT	N	193.1	-17.8	6	19.4	
	HT	275-290	Y	63.1	61	2	1.1	
D194c.1	LC	2-10 mT	N	45.3	22.4	5	24.9	No origin-trending component
D194c.2	LC	2-10 mT	N	72.4	3.1	5	34.2	
	LT	80-250°C	N	351.2	-64.2	8	21.4	
	HT	290-510°C	Y	357.4	62	10	11.5	
D194c.3	LC	2-10 mT	N	41.3	-14.2	5	31.3	
	LT	100-360°C	N	64.1	-17.9	12	15.9	
	HT	400-520°C	Y	17.4	72.3	8	13.2	
D195a.1	HT	225-360°C	Y	3.8	61	7	0.7	
D195a.2	HT	275-360°C	Y	4.4	61.7	5	0.7	
D195a.3	HT	290-360°C	Y	2.5	62	4	0.8	
D195b.1	LT	NRM-125°C	N	328	-67	9	11.5	
	HT	225-320°C	Y	1.6	52	6	3.7	
D195b.2	HT	200-320°C	Y	0.1	50.3	7	4.3	
Quartzite mean	LT			46.2	-41.8	10	38.1	Fisher k = 2.3
Quartzite mean	HT			9.3	61.2	10	8.8	Fisher k = 27.7

Fold Tests:

D102:								
D102a.1	LT	NRM-200°C	N	52.6 79	1.4 27.6	9	16.6	
	HT	200-325°C	Y	59.9 28	-49.3 9.5	5	2.9	
D102b.1	LT	NRM-200°C	N	167.6 138.9	50.8 1.5	9	8.7	
	HT	275-350°C	Y	354.8 66.8	55.3 29	3	1.8	
D102b.2	LT	NRM-200°C	N	204.4 130.7	65.9 24.2	9	13.7	
	HT	275-350°C	Y	350.3 71.2	59 31.2	4	1.9	
D102b mean	HT			352.7 69	57.2 30.1	2		
D102c.1	LT	4 mT-200°C	N	41.6 13.3	-19.7 -12.9	7	6.5	

D102c.3	LT	4 mT-150°C	N	46.2 8.3	-24.8 -17.4	6	12.9	
D102d.1	LC	NRM-10 mT	N	281.5 276.1	43.1 -33	6	9.6	
	LT	200-325°C	N	10.2 53.4	-75.3 4.3	5	4.1	
	MT	325-400°C	N	320.4 319.3	14.7 -13.4	3	1.4	
	HT	400-662°C	Y	115.7 89.7	-59.1 15.5	17	26.6	
D102d.3	LT	150-325°C	N	347.1 30.6	-54.3 3.4	6	8.8	
	MT	325-400°C	N	285.4 36.7	-50.8 -32.6	3	11	Using second 275°C step
	HT	400-475°C	Y	38.7 331.3	5.5 63.2	3	22	
D102d mean	HT			62.9 61.8	-32 53.8	2		
D102e.1	LT	4 mT-275°C	N	145.4 264.3	-35 -48.6	9	10.3	
	HT	275-350°C	Y	183 267.5	-56.6 -15.4	4	12	
D102e.3	LT	4 mT-200°C	N	108 314.5	-34 -56.5	7	9	
	HT	250-325°C	Y	190.4 248.3	-38.8 -15.3	4	9.7	
D102e mean	HT			187.3 257.9	-47.8 -15.6	2		
D102f.1	LT	NRM-200°C	N	87.2 94.6	12.7 -2.7	9	3	
	HT	200-325°C	Y	108.9 123.9	36.1 -11.9	5	3.5	
D102 HT mean				80.5 66.8	-17 28.9	5	118.7 117.2	Fisher k_{geo} = 1.1 Fisher k_{tilt} = 1.1
D197:								
D197a.1	LT	NRM-100°C	N	41.5 92.6	-45.9 -27.9	7	17	
	MT	100-350°C	N	330.7 6.6	-21.6 -81.5	9	13.4	
	HT	350-640°C	Y	346.7 50	-24.6 -69.9	17	0.8	
D197b1.1	LT	4 mT-300°C	N	102.1 19.6	47.7 67	9	27.6	
	MT	300-325°C	N	4.9 350.4	39.9 4.3	2		2 point fit
	HT	350-640°C	Y	340.3 78.4	-50.8 -69.7	17	13.4	
D197b2.1	MT	250-325°C	N	351 313.3	40 45	4	4.3	
	HT	325-640°C	Y	157.2 192.9	55.3 34.4	18	2.4	

D197c.1	LT	NRM-250°C	N	85.8 85.9	-15.6 15.3	10	20.1	
	MT	250-325°C	N	342.1 339.6	43.5 -21.6	4	2.8	Origin-trending; Labeled MT because similar temperature range to MT components of other samples; Using second 275°C step
D197d.1	LT	NRM-100°C	N	84.3 92.3	-66.5 -36.2	7	18.5	
	MT	100-325°C	N	354 358.5	-4.6 -11.8	7	10.8	
	HT	350-640°C	Y	70 88.4	-73.7 -44.2	17	2.4	
D197d.2	LT	NRM-100°C	N	154.1 132.6	-55.1 -31.9	7	14.2	
	MT	100-350°C	N	334.1 337.3	1.9 -15.7	8	6.4	Using first 275°C step
	HT	350-640°C	Y	72 91	-77.6 -47.7	17	4.6	
D197d mean	MT			344 348	-1.4 -14	2		
	HT			70.9 89.7	-75.7 -45.9	2	8.6	
D197 mean	MT			345.8 340.9	21 -12.7	5	32 49.5	Fisher k_{geo} = 5.4 Fisher k_{tilt} = 2.5
D197 mean	HT			1.8 114.6	-52.2 -58.9	4	90 92.6	Fisher k_{geo} = 1.0 Fisher k_{tilt} = 1.4
Erawandoo Hill pebble conglomerates (clast and matrix samples):								
EHJH5:								
0h	LT	NRM-200°C	N	74.8	-83.2	4	8.8	Clast
	HT	250-325°C	Y	334	11.6	4	11.2	
0i	LT	150-275°C	N	59.1	17.5	4	19	Clast
	HT	275-335°C	Y	339.2	19	4	3.5	
0j	LT	NRM-250°C	N	36	1.1	5	13.9	Clast
	HT	300-335°C	Y	333.4	14.4	3	5.1	
0k	LT	NRM-250°C	N	155.5	44.7	5	19.4	Clast
	HT	275-335°C	Y	351.5	-21.6	4	18.4	
2aa	HT	275-335°C	Y	318.8	-4.4	4	2.7	Clast
2ab	LT	NRM-250°C	N	235.2	-75.8	5	18.4	Clast
	HT	275-325°C	Y	319.7	30	3	4.6	
2c	LT	NRM-250°C	N	63.5	-12.9	5	8.5	Clast
	HT	300-325°C	Y	338.7	-7.6	2	9.4	
2e	HT	250-335°C	Y	345.2	31.4	5	3.2	Clast
2f	LT	NRM-250°C	N	35.9	-38.2	5	13.7	Clast
	HT	300-335°C	Y	350.4	39.3	3	3.3	
2j	LT	NRM-275°C	N	329	-17.5	6	12.2	Clast
	HT	275-345°C	Y	323.1	35.8	5	13	
2l	LT	NRM-200°C	N	130.2	-8.5	4	5.2	Clast
	HT	250-325°C	Y	326.9	-3.7	4	8.4	

3f	HT	75-395°C	Y	337.6	34.8	14	5.6	Clast
3g	HT	250-335°C	Y	334.2	6.3	5	6.9	Clast
3j	HT	300-345°C	Y	312.5	9.2	4	14.2	Clast
3k	LT	150-275°C	N	333.5	-19.5	4	8.6	Clast
	HT	275-335°C	Y	326.2	51.6	4	5	
3m	HT	250-335°C	Y	343.8	21.9	6	3.8	Clast
4a	HT	200-325°C	Y	321.5	24	5	10.1	Clast
4e	HT	200-335°C	Y	328	9	6	5.2	Clast
4f	HT	250-335°C	Y	331.6	25.3	5	4.4	Clast
4h	LT	NRM-275°C	N	340.3	-35.1	6	7.4	Clast
	HT	275-335°C	Y	324.4	5.8	4	5.1	
4i	LT	NRM-150°C	N	334.5	-52.5	3	0.8	Clast
	HT	150-325°C	Y	303.4	-22.4	6	19.2	Noisy demagnetization
4k	HT	250-335°C	Y	326.1	1.6	5	1.7	Clast
4l	HT	250-355°C	Y	328.5	-5.1	7	1.7	Clast
4m.1	LT	NRM-200°C	N	104	1.2	4	32.4	Clast
	MT	200-325°C	N	227.7	0.5	5	23.7	
	HT	325°C	Y	353.6	15.5	1		Single point plus origin
4m.2	LT	NRM-200°C	N	297.6	16.4	4	1.4	
	HT	200-300°C	Y	330.9	1.2	4	13	Clast
4m clast mean	HT			342	8.5	2	61.5	
5c	LT	150-275°C	N	309.1	-36.6	4	10.4	Clast
	HT	300-335°C	Y	334	22.8	3	2.6	
5e	LT	150-250°C	N	41.7	-5.5	3	17.6	Clast
	HT	275-325°C	Y	337.1	16.1	3	2.6	
5f	LT	NRM-150°C	N	344.3	-57.3	3	0.9	Clast
	HT	200-325°C	Y	30.3	28.7	5	5.5	
5g.1	LT	250-300°C	N	310.3	25.1	3	8.3	Clast
	HT	300-325°C	Y	314.7	-41.3	2	4.8	
5g.2	HT	250-325°C	Y	321.2	23.6	4	6	Clast
5g clast mean	HT			318.3	-8.9	2	90	
5h	LT	NRM-200°C	N	27.9	52.4	4	3.5	Clast
	HT	250-325°C	Y	325.1	1.9	4	4.5	
5i	LT	NRM-200°C	N	242	-47.4	4	7.8	Clast
	HT	275-300°C	Y	338	-17.1	2	4.3	
5j				No stable magnetization (clast)				
s1f	LT	NRM-200°C	N	335.5	-54.4	4	2.7	Matrix
	MT	200-325°C	N	21.1	2.5	5	3.4	
	HT	325-625°C	Y	5.5	-29.3	14	16	
s1h	LT	250-335°C	N	355.5	8.9	5	3.9	Matrix
	HT	335-625°C	Y	38.4	1.3	13	2.4	Not fully demagnetized
s2b	LT	NRM-150°C	N	325.8	-24	3	2.6	Matrix
	HT	275-625°C	Y	359	-5.4	15	6.7	Not fully demagnetized
s2k.1	LT	NRM-325°C	N	19.7	19.6	8	7.1	Matrix
	HT	325-625°C	Y	37.6	8	13	6.1	Not fully demagnetized
s2k.2	LT	NRM-150°C	N	201.1	-29.7	3	1.6	Matrix
	MT	150-345°C	N	20.5	24.3	8	6.4	

	HT	345-660°C	Y	38.1	7.4	13	6.5	
s3a	LT	NRM-150°C	N	352.1	-37.1	3	2.3	Matrix
	MT	150-335°C	N	334	47.2	7	8.9	
	HT	335-660°C	Y	32.7	35.8	14	5.1	
s3g	MT	150-335°C	Y	352.7	27.8	7	5.9	Matrix
EHJH5 clast/matrix mean	LT			1.9	-33.4	26	31.6	Fisher k = 1.8
EHJH5 clast mean	HT			332.3	12.3	30	7.9	Fisher k = 12.2, R = 27.6
EHJH6:								
a2m	LT	50-175°C	N	215.4	10.8	4	6.5	Matrix
	HT	175-335°C	Y	265	55.2	14	11.7	
a3m	No stable magnetization (matrix)							
a4m	HT	50-200°C	Y	334.7	60.6	5	1.7	Matrix
a5m	LT	NRM-150°C	N	209.8	3.7	4	20.1	Matrix
	HT	150-200°C	Y	35.9	47.3	3	8.2	
a6m	LT	100-175°C	N	268.5	43.4	3	10.2	Matrix
	HT	175-335°C	Y	0.3	72.3	13	31.2	
a7m	LT	50-150°C	N	236.8	3.2	3	17.5	Matrix; No origin-trending HT component
a8c	No stable magnetization (clast)							
a9c	LT	NRM-150°C	N	135.3	21.7	4	9.4	Clast
	HT	*150-275°C*	*Y*	*164.8*	*16.3*	*9*	*28.2*	*Ambiguous fit*
a10c	LT	50-150°C	N	270.3	0	3	4.7	Clast
	HT	150-225°C	Y	359.5	48.1	4	9.7	
a11c	LT	NRM-175°C	N	204	38.9	5	16.1	Clast
	HT	225-275°C	Y	17	40.3	6	6.2	
a12c	LT	50-200°C	N	281.6	-25.9	5	13.7	Clast
	MT	200-255°C	N	78.7	25.1	5	27.3	Ambiguous fit; no origin-trending HT component
a13c	HT	175-325°C	Y	283.2	63	13	9	
a15ac	LT	NRM-235°C	N	244	-32.2	8	7.6	Clast
	MT	255-315°C	N	100.6	48.1	8	10.1	No origin-trending HT
a15bc	LT	NRM-235°C	N	136.4	-64	8	39.9	Clast
	MT	265-285°C	N	303	38.4	3	3.6	
	HT	285-335°C	Y	10.5	49	6	10.5	
a16c	LT	100-265°C	N	238.5	-39.7	9	13.1	Clast
	HT	265-335°C	Y	246.7	17.4	8	5.4	
a17c	LT	NRM-265°C	N	181.8	-45.1	11	16.2	Clast
	HT	265-335°C	Y	236.7	6.6	8	1.9	
a18c	LT	NRM-305°C	N	200.6	-34.6	15	25	Clast
	HT	305-345°C	Y	23.6	48.6	5	2.8	
c01c	LT	50-175°C	N	309.6	3.7	4	4.3	Clast

	HT	*175-335°C*	*Y*	*196.4*	*-54.5*	*12*	*13*	*Not completely demagnetized*
c02c	LT	100-225°C	N	265.8	-4.5	5	18.4	Clast; ambiguous fit; weak moment; no origin-trending HT component
c03c	LT	50-200°C	N	125.7	-4.6	5	9.6	Clast; no origin-trending HT
c04m	LT	NRM-100°C	N	45.5	-54.4	3	19.9	Matrix; ambiguous fit
	HT	100-250°C	Y	253.2	61.1	6	13.8	
c05c.1	LT	NRM-225°C	N	235.2	18.1	7	11.5	Clast; no origin-trending HT component
c05c.2	LT	NRM-175°C	N	91.1	33.5	5	37.4	Clast; Ambiguous fit; no origin-trending HT component
c05c.3	LT	100-175°C	N	296.6	35.8	3	10	Clast; no origin-trending HT component
c05c.4	LT	NRM-100°C	N	349	16.9	3	1.7	Clast
	MT	150-200°C	N	23.5	-43.7	3	3	
c07m	LT	150-200°C	N	20.7	48.9	3	2.3	Matrix
	HT	200-225°C	Y	4.4	66.1	2	6.9	Two point fit
c08c	No stable magnetization (clast)							
c09m	LT	50-175°C	N	322.5	59.8	4	8.5	Matrix
	HT	200-335°C	Y	211.6	60.7	11	5.3	Not fully demagnetized
c10c	LT	NRM-200°C	N	270.8	-33	6	36.3	Clast; ambiguous fit
	HT	200-225°C	Y	46.7	49.4	2	2.6	Two point fit
c11c.1	LT	NRM-150°C	N	320.9	-1.7	4	2.9	Clast; no origin-trending HT component
c11c.2	LT	175-200°C	N	179.8	-58.3	2		Clast; two point fit; no origin-trending HT component
c11c.3	LT	NRM-200°C	N	304.4	-6	6	11.7	Clast; no origin-trending HT component
c11c.4	LT	100-200°C	N	245.3	64.5	4	11.4	Clast; ambiguous fit; no origin-trending HT component
c11c.5	LT	NRM-200°C	N	148.9	54.7	6	5.1	Clast
	MT	200-350°C	Y	262.7	-66.1	12	36	Ambiguous fit; no origin-trending HT component
c12m	LT	NRM-225°C	N	124.9	0.6	7	14.9	Matrix
	HT	225-335°C	Y	245.3	37.1	10	2.7	
c13m	LT	100-285°C	N	217	-5.3	9	15.2	Clast
	HT	285-335°C	Y	21.2	50.1	6	2.7	Matrix
c14m	HT	305-335°C	Y	358.5	52.9	4	5.4	Matrix
c15m	HT	200-325°C	Y	239.5	25.6	10	1.4	Matrix
c16c	HT	100-265°C	Y	229.9	23.3	7	2.8	Clast
c20m	LT	NRM-100°C	N	26.3	-57.2	3	5.3	Matrix
	HT	100-200°C	Y	121.2	29.5	4	7.8	
c21c	HT	100-200°C	Y	336.5	56.7	4	3.4	Clast
c22c.1	No stable magnetization (clast)							
c22c.2	No stable magnetization (clast)							
c24m	LT	150-225°C	N	2.4	59	4	8.2	Matrix
	HT	*225-500°C*	*Y*	*202.4*	*42.5*	*14*	*5.7*	*Not fully demagnetized*

c26m	LT	50-175°C	N	257.5	0.4	4	28.2	Matrix
	HT	*175-500°C*	*N*	*219.2*	*51.7*	*16*	*13.9*	*Not fully demagnetized*
EHJH6 clast/matrix mean	LT			244.7	8.7	34	34.3	Fisher *k* = 1.5
EHJH6 clast/matrix mean	HT			312	72.5	22	19	Fisher *k* = 3.5
EHJH7:								
a01m	LT	NRM-150°C	N	313.2	-11.5	4	8.1	Matrix
	MT	150-250°C	N	49.5	85.3	4	11.9	
	HT	250-350°C	Y	315.4	-6.4	10	23.5	Ambiguous
a02m	LT	NRM-150°C	N	318.6	-2.6	4	6.2	Matrix
	HT	150-500°C	Y	289	16.3	17	19.1	Not fully demagnetized
a03m	LT	100-225°C	N	355.7	28.2	5	19.9	Matrix
	HT	225-450°C	Y	334.4	-16.9	13	26.4	
a04c	LT	NRM-150°C	N	325.8	19.9	4	7.2	Clast
a05m				No stable magnetization (matrix)				
a06m	LT	100-265°C	N	328.5	36	7	12.5	Matrix
	HT	275-335°C	Y	333	13.4	7	22.7	
a07m	LT	150-250°C	N	323.6	9.3	5	6.9	Matrix
	HT	250-325°C	Y	41.1	0.1	8	23.9	
a08c.1	LT	150-250°C	N	340.5	-18.7	5	5	Clast
	HT	250-400°C	Y	355.5	-23.1	11	17.3	Not fully demagnetized
a08c.2	LT	200-250°C	N	355.4	-45.1	3	1.2	Clast
	HT	250-450°C	Y	335.7	-18	13	12.8	
a08c.3	LT	175-225°C	N	347.6	-16.1	4	10.9	Clast
	HT	315-500°C	Y	343.3	-10.4	7	7.3	Not fully demagnetized
a08c clast mean	HT			344.7	-17.3	3	17.5	Mean of subsamples 1, 2, and 3
a09c.1	LT	NRM-315°C	N	26	-2.7	14	7.8	Clast
	MT	315-335°C	N	51.6	69.1	3	8	
	HT	335-500°C	Y	19.4	-5.7	5	7.6	
a09c.2	HT	250-325°C	Y	341.2	-3	8	3.6	
a09c.3				No stable magnetization (clast)				
a09c clast mean	HT			0.3	-4.6		74.1	Mean of subsamples 1 and 2
EHJH7 clast/matrix mean	LT			338.7	-0.2	10	20.1	Fisher *k* = 5.7
EHJH7 clast/matrix mean	HT			342.6	-6.2	10	21.1	Fisher *k* = 5.6
Cobble conglomerates (all samples are from clasts):								
D107c.2	LC	NRM-6 mT	N	237.8	-51.8	4	10.3	
	MT	150-325°C	N	89.4	-13.3	6	15.3	
	HT	325-662°C	Y	34.5	-65.3	17	21.7	Hematite carrier
D107c.3	LT	NRM-200°C	N	137.8	-81.7	9	5.6	
	MT	275-350°C	N	100.1	-28.7	4	6	

	HT	350-600°C	Y	18.1	-57	13	21	Hematite carrier
D107c clast mean	MT			94.5	-21.1	2	41	Mean of subsamples 2 and 3
D107c clast mean	HT			25.2	-61.4	2	25.1	
D107g.1	LT	NRM-100°C	N	202	-3.4	7	7.1	
	HT	100-560°C	Y	174.7	21	17	5.3	
D107h.1	LT	4 mT-275°C	N	216.3	53.6	9	11.9	
	HT	275-325°C	Y	143.8	55.8	3	4.7	
D107i.1	LT	6 mT-275°C	N	206.2	52	8	3.9	
	HT	275-325°C	Y	182.8	67.5	3	3.3	Not clearly origin-trending
D108.1	LT	4 mT-275°C	N	265.9	8.9	9	11.1	
	HT	275-325°C	Y	236.1	6	4	6.4	
D108.2	LT	4 mT-275°C	N	271.5	-3.1	9	15.7	
	HT	275-325°C	Y	251.6	-10.3	3	4.1	
D108 clast mean	HT			243.8	-2.2	2		Mean of subsamples 1 and 2
D109a.1	LT	2-10 mT	N	255	57.3	5	6.6	
	HT	150-565°C	Y	216.8	-43.5	18	2.6	
D109b.1	HT	4 mT-325°C	Y	108	-48.5	11	1.5	
D109b.2	HT	4 mT-570°C	Y	105.2	-46.6	25	2.1	Suspect HT component: low minimum blocking temperature
D109b clast mean	HT			106.6	-47.5	2		Mean of subsamples 1 and 2
D110.1	LT	4 mT-250°C	N	268.4	-48.2	8	12.4	
	HT	275-300°C	Y	276.5	-43.5	2	3.1	
D111c.45				No stable magnetization				
D111c.6				No stable magnetization				
D111d.2	LC	6-10 mT	N	221.5	13.4	3	3.5	
	LT	10 mT-250°C	N	12	48.3	5	19.3	
	MT	250-325°C	N	48.9	-22.3	4	6.6	No origin-trending HT component
D111d.3	LT	NRM-150°C	N	192.1	-48.5	8	21.5	
	MT	150-250°C	N	110.9	-23.5	3	12.5	No origin-trending HT component
D111e.2	LC	NRM-10 mT	N	152.2	10.5	6	12.4	
	LT	10 mT-300°C	N	44.4	36.3	7	15.2	No origin-trending HT component
D111e.3	LT	6 mT-200°C	N	59.8	45.8	6	20.6	
	MT	200-250°C	N	112.8	-70.7	2		2 point fit; No origin-trending HT component
D111h.1	LC	NRM-6 mT	N	304.8	-37.8	4	11.9	No origin-trending HT component
D111h.2	LC	2-8 mT	N	260.4	-30.3	4	19.7	
	LT	8 mT-275°C	N	107.9	4.1	7	30.5	No origin-trending HT component
D111i.5	LT	NRM-150°C	N	74.6	40	8	35.1	No origin-trending HT component
D111i.6	LT	6 mT-250°C	N	2	-12.8	7	15.9	
	HT	275-325°C	Y	214.1	4.8	3	13	Inhomog. with subsample 5
D111j.1	LT	NRM-250°C	N	97.8	-41	10	15.2	No origin-trending HT component
D111j.2	LT	NRM-200°C	N	96.7	13.1	9	13.6	
	MT	200-300°C	N	41	-1.1	4	30.4	No origin-trending HT component
D112c.1	LT	8 mT-275°C	N	84.8	16.1	7	17.4	No origin-trending HT component
D112c.2	LC	2-6 mT	N	164.7	-43.1	3	7.3	

	LT	6 mT-200°C	N	100.9	-8.7	6	21.5	No origin-trending HT component
D112d.1	LT	8 mT-275°C	N	293.6	6.9	7	26.1	No origin-trending HT component
D112d.3	LC	NRM-6 mT	N	262.2	-28.1	4	3.7	
	LT	6 mT-250°C	N	266.6	39	7	11.3	No origin-trending HT component
D112e.2	LT	8 mT-250°C	N	115.5	-26.7	6	18.1	
	MT	250-300°C	N	16.9	39.7	3	8.2	No origin-trending HT component
D112f.1	LC	NRM-4 mT	N	261.5	-32.8	3	14.4	
	LT	4 mT-275°C	N	94.4	-37	9	21.1	
	HT	275-325°C	Y	231.9	1.6	3	12.6	Not clearly origin-trending
D112g.1	LC	NRM-10 mT	N	186.8	-1.2	6	15.7	
	LT	100-250°C	N	34.6	59.5	4	33.4	Ambiguous; no origin-trending
D112g.2	LC	2-10 mT	N	71.8	72.4	5	32.8	
	LT	200-275°C	N	71	-16.6	3	29.6	
	MT	275-350°C	N	260.4	-8	4	19.2	No origin-trending HT component
D112j.2	LT	NRM-150°C	N	253.8	-62.6	8	20.1	
	MT	150-275°C	N	234.5	69.9	4	13.4	No origin-trending HT component
D112j.3	LT	8 mT-200°C	N	240.2	15.4	5	40	
	MT	200-275°C	N	75.8	38.9	3	19.9	No origin-trending HT component
D112k.3	LT	250-325°C	N	148.6	65.2	4	9.8	No origin-trending HT component
D112k.4	LT	150-250°C	N	166.6	32.3	3	8.5	No origin-trending HT component
D112l.1	LC	2-10 mT	N	205.4	69.3	5	16.9	No origin-trending HT component
D112l.2	LT	8 mT-275°C	N	112.8	19	7	33.3	No origin-trending HT component
D192c.1					No stable magnetization			
W025a.2	LT	NRM-250°C	N	84.2	-44.9	10	14.2	No origin-trending HT component
W025a.3	LC	NRM-10 mT	N	93.6	-33.3	6	29.2	No origin-trending HT component
W025b.1	LT	NRM-150°C	N	46.7	-1.7	8	4.4	No origin-trending HT component
W025b.3	LT	NRM-150°C	N	4.1	-46.8	8	6.3	No origin-trending HT component
W025c.3	LC	NRM-10 mT	N	115.3	7.1	6	6.7	
	LT	10 mT-250°C	N	253.5	4.6	5	24.7	No origin-trending HT component
W025c.4	LC	NRM-10 mT	N	122.4	-3.5	6	8.1	
	LT	10 mT-200°C	N	229.8	72.7	4	9.4	No origin-trending HT component
W025d.f1	LT	NRM-150°C	N	184.4	-73.6	8	3.6	No origin-trending HT component
W025f.4	LC	NRM-8 mT	N	20.5	-2.1	5	3.6	
	MT	8 mT-200°C	N	156.5	-43.3	5	4.7	No origin-trending HT component
W025f.5	LC	NRM-10 mT	N	1.1	-48.7	6	16.2	
	LT	10 mT-250°C	N	152.3	-34.1	5	17.2	
	MT	275-350°C	N	276.7	14.1	4	29.9	No origin-trending HT component
W025g.2	LC	NRM-8 mT	N	167.6	-1	5	3.7	
	LT	10 mT-275°C	N	316.6	74.2	6	36.2	No origin-trending HT component
W025g.4	HT	100-300°C	Y	13.1	72	6	13.6	Inhomogeneous with subsample g.2; Weak moment
W025h.2	LC	NRM-6 mT	N	208.8	-5.9	4	9.6	
	LT	6 mT-200°C	N	30.1	-2.6	6	17.7	No origin-trending HT component

W025h.3	LC	NRM-10 mT	N	77.3	-3	6	22.5	No origin-trending HT component
W025i.2	LT	4 mT-325°C	N	118.1	35.1	11	15.3	
	HT	325-450°C	Y	270	-36	4	28.7	Not present in subsample i.3
W025i.3	LC	NRM-6 mT	N	69.6	-74.6	4	1.8	
	LT	6 mT-200°C	N	98.7	-37.3	6	9.7	
	MT	250-350°C	N	112.1	44.9	5	20.8	No origin-trending HT component
W025j.1	HT	8 mT-400°C	Y	95.8	18.1	11	2.1	
W025j.2	HT	100-350°C	Y	96.3	18.5	8	2.8	
W025j clast mean	HT			96	18.3	2	1.4	Mean of subsamples 1 and 2
W025k.3	HT	6 mT-560°C	Y	272.7	-22.9	20	8.9	
W025k.4	HT	6 mT-580°C	Y	270.5	-25.5	22	12.2	
W025k clast mean	HT			271.6	-24.2	2	7.2	Mean of subsamples 3 and 4
W025l.1	LC	NRM-10 mT	N	319	-31	6	7.2	
	HT	10 mT-300°C	Y	347.1	-43.1	7	5.6	
W025l.2	LT	4 mT-100°C	N	3.6	-36.1	5	0.9	
	MT	100-325°C	N	352.9	-36.9	7	16.9	
	HT	325-640°C	Y	331.7	-31.4	18	21.3	Hematite carrier
W025l clast mean				350.1	-40.1	2		Combining HT for subsample 1 with MT for subsample 2
W026.4	HT	4 mT-300°C	Y	30.3	-46.5	10	4.7	
W026.5	HT	4 mT-300°C	Y	36.1	-60.9	10	13.8	
W026 clast mean	HT			32.7	-53.7	2	32.8	Mean of subsamples 4 and 5

Note: The first column gives the sample name (samples with the same name before the period are from the same block/clast), the second column lists the component name, the third column lists the coercivity range or blocking temperature range, the fourth column denotes whether the PCA fit was anchored to the origin, the fifth column gives the declination, the six column gives the inclination, the seventh column gives the number of samples, the eighth column gives the maximum angular deviation (for individual fits) or 95% confidence intervals (for the means), and the final column gives notes and estimated Fisher *k* precision parameters. For all samples except fold test samples, inclination and declination are in geographic (i.e., in situ) coordinates. For fold test samples, top and bottom rows of inclination and declination give geographic and bedding-corrected coordinates, respectively. *Italicized* measurements were considered unreliable and are excluded from calculated mean values at the bottom of each subsection and from paleomagnetic field tests. All fits are line fits except for the great circle fit denoted by an asterisk (for which the pole location is listed in columns five and six).

Table S3. Peak unblocking temperatures for components oriented toward the Warakurna LIP local paleomagnetic field direction.

Sample	Lithology	Peak Temperature (°C)
BC0	dolerite	585
BC1	dolerite	585
Dol1	dolerite	560
Dol2	dolerite	530
Dol3	dolerite	585
Dol5	dolerite	530
D154d	dolerite	585
BCB2	quartzite near dolerite	510
BCB3	quartzite near dolerite	450
BCB4	quartzite near dolerite	575
BCB5	quartzite near dolerite	565
BCB6	quartzite near dolerite	520
BCB8	quartzite near dolerite	510
BCB10	quartzite near dolerite	575
BC3	quartzite near dolerite	225
BC4	quartzite near dolerite	585
BC6	quartzite near dolerite	565
BC7	quartzite near dolerite	570
BC8	quartzite near dolerite	560
BC9	quartzite near dolerite	560
BC10	quartzite near dolerite	360
D154c	quartzite near dolerite	500
D154e	quartzite near dolerite	565
D154f	quartzite near dolerite	520
D154g	quartzite near dolerite	560
D154h	quartzite near dolerite	225
D154i	quartzite near dolerite	320
D182a	monzogranite	290
D183	monzogranite	560
D184	monzogranite	575
D185	monzogranite	480
D186	monzogranite	540
D187	monzogranite	540
D188	monzogranite	320
Blob4a	monzogranite	520
Blob5b	monzogranite	520
Blob5c	monzogranite	520
D192b	quartzitic rock distal to dyke	360
D194c	quartzitic rock distal to dyke	520

D195a	quartzitic rock distal to dyke	360
D195b	quartzitic rock distal to dyke	320
D197a	quartzitic rock distal to dyke	350
D197b1	quartzitic rock distal to dyke	325
D197b2	quartzitic rock distal to dyke	325
D197c	quartzitic rock distal to dyke	325
D197d	quartzitic rock distal to dyke	350
EHJH5	Erawandoo Hill conglomerate clasts	345
EHJH5	Erawandoo conglomerate matrix	660
EHJH6	Erawandoo Hill conglomerate clasts	335
EHJH6	Erawandoo conglomerate matrix	335
EHJH7	Erawandoo Hill conglomerate clasts	>500
EHJH7	Erawandoo conglomerate matrix	450

Note: The first column gives the sample name, the second column lists the sample lithology, and the third column lists the peak unblocking temperatures of magnetization directions oriented like that of the local paleomagnetic field at 1070 Ma during the emplacement of the Warakurna LIP. When multiple subsamples of a given subsample were analyzed, the maximum unblocking temperature among the subsamples is shown here.

Supplementary References

Bowring, J.F., McLean, N.M., Bowring, S.A., 2011. Engineering cyber infrastructure for U-Pb geochronology: Tripoli and U-Pb_Redux. Geochem. Geophys. Geosyst. 12, Q0AA19.

Dunlop, D.J., Özdemir, O., 1997. Rock magnetism: Fundamentals and frontiers. Cambridge University Press, New York. 573 pp.

Dunlop, D.J., 2002. Theory and application of the Day plot (M_{rs}/M_s versus H_{cr}/H_c) - 1. Theoretical curves and tests using titanomagnetite data. J. Geophys. Res. 107, doi:10.1029/2001JB000486.

Jaffey, A.H., Flynn, K.F., Glendenin, L.E., Bentley, W.C., Essling, A.M., 1971. Precision measurement of half-lives and specific activities of ^{235}U and ^{238}U. Phys. Rev. C 4.

Li, H.-Y., Zhang, S.-H., 2005. Detection of mineralogical changes in pyrite using measurements of temperature-dependence suscpetibilities. Chinese Journal of Physics 48, 1454-1461.

Mattinson, J.M., 2005. Zircon U/Pb chemical abrasion (CA-TIMS) method; combined annealing and multi-step partial dissolution analysis for improved precision and accuracy of zircon ages. Chem. Geol. 220, 47-66.

McClean, N.M., Bowring, J.F., Bowring, S.A., 2011. An algorithm for U-Pb isotope dilution data reduction and uncertainty propagation. Geochem. Geophys. Geosyst. 12, Q0AA18.

Myers, J.S., 1995. The generation and assembly of an Archaean supercontinent: Evidence from the Yilgarn craton, Western Australia. J. Geol. Soc. London Spec. Pub. 95, 143-154.

Pidgeon, R.T., 1992. Recrystallisation of oscillatory zoned zircon: Some geochronological and petrological implications. Contrib. Mineral. Petrol. 110, 463-472.

Pidgeon, R.T., Wilde, S.A., 1998. The interpretation of complex zircon U–Pb systems in Archaean granitoids and gneisses from the Jack Hills, Narryer Gneiss Terrane, Western Australia. Precambrian Res. 91, 309-322.

Pidgeon, R.T., 2014. Zircon radiation damage ages. Chem. Geol. 367, 13-22.

Ramezani, J., Hoke, G.D., Fastovsky, D.E., Bowring, S.A., Therrien, F., Dworkin, S.I., Atchley, S.C., Nordt, L.C., 2011. High-precision U-Pb zircon geochronology of the Late Triassic Chinle Formation, Petrifi ed Forest National Park (Arizona, USA): Temporal constraints on the early evolution of dinosaurs. Geol. Soc. Am. Bull. 123, 2142–2159.

Rasmussen, B., Fletcher, I.R., Muhling, J.R., Wilde, S.A., 2010. In situ U–Th–Pb geochronology of monazite and xenotime from the Jack Hills belt: Implications for the age of deposition and metamorphism of Hadean zircons. Precambrian Res. 180, 26-46.

Rasmussen, B., Fletcher, I.R., Muhling, J.R., Gregory, C.J., Wilde, S.A., 2011. Metamorphic replacement of mineral inclusions in detrital zircon from Jack Hills, Australia: Implications for the Hadean Earth. Geology 39, 1143-1146.

Roberts, A.P., Cui, Y., Verosub, K.L., 1995. Wasp-waisted hysteresis loops: Mineral magnetic characteristics and discrimination of components in mixed magnetic systems. J. Geophys. Res. 100, 17909-17924.

Spaggiari, C.V., 2007. The Jack Hills greenstone belt, Western Australia Part 1: Structural and tectonic evolution over >1.5 Ga. Precambrian Res. 155, 204-228.
Spaggiari, C.V., Wartho, J.-A., Wilde, S.A., 2008. Proterozoic deformation in the northwest of the Archean Yilgarn Craton, Western Australia. Precambrian Res. 162, 354-384.
Tarduno, J.A., Cottrell, R.D., 2013. Signals from the ancient geodynamo: A paleomagnetic field test on the Jack Hills metaconglomerate. Earth Planet. Sci. Lett. 367, 123-132.
Tudryn, A., Tucholka, P., 2004. Magnetic monitoring of thermal alteration for natural pyrite and greigite. Acta Geophysica Polonica 52, 509-520.
Wang, L., Pan, Y.X., Li, J.H., Qin, H.F., 2008. Magnetic properties related to thermal treatment of pyrite. Science in China D 51, 1144-1153.
Wang, X.-C., Li, Z.-X., Li, J., Pisarevsky, S.A., Wingate, M.T.D., 2014. Genesis of the 1.21 Ga Marnda Moorn large igneous province byplume–lithosphere interaction. Precambrian Res. 241, 85-103.
Wingate, M.T.D., Pirajno, F., Morris, P.A., 2004. Warakurna large igneous province: A new Mesoproterozoic large igneous province in west-central Australia. Geology 32, 105-108.